

# A statistical study of ionospheric profile parameters derived from Millstone Hill incoherent scatter radar measurements

Jiuhou Lei,<sup>1,2,3</sup> Libo Liu,<sup>1</sup> Weixing Wan,<sup>1</sup> Shun-Rong Zhang,<sup>4</sup> and John M. Holt<sup>4</sup>

Received 22 May 2004; revised 14 June 2004; accepted 18 June 2004; published 24 July 2004.

[1] Diurnal, seasonal, and solar activity variations of the bottomside electron density profile parameters  $B0$  and  $B1$ , representing the F2 layer thickness and shape, are studied using a large incoherent scatter radar dataset for Millstone Hill covering the period 1976–2002. These results are compared with the latest IRI model. Our statistical study is characterized by morning and afternoon falls in the diurnal variation of  $B0$  for seasons other than summer and a  $\sim 15\%$  change in  $B1$  over a solar cycle, features not fully well represented by the standard IRI model. The standard IRI  $B1$ , however, is very close to observations in terms of the diurnal variation. **INDEX TERMS:** 2443 Ionosphere: Midlatitude ionosphere; 2447 Ionosphere: Modeling and forecasting; 6929 Radio Science: Ionospheric physics (2409); 6952 Radio Science: Radar atmospheric physics. **Citation:** Lei, J., L. Liu, W. Wan, S.-R. Zhang, and J. M. Holt (2004), A statistical study of ionospheric profile parameters derived from Millstone Hill incoherent scatter radar measurements, *Geophys. Res. Lett.*, *31*, L14804, doi:10.1029/2004GL020578.

## 1. Introduction

[2] The International Reference Ionosphere (IRI) model is the most widely used empirical ionospheric model and is recognized as the standard specification of ionospheric parameters by the Committee on Space Research (COSPAR) and the International Union of Radio Science (URSI). Over the past two decades, this model has undergone periodic revisions [Rawer *et al.*, 1978; Rawer, 1990; Bilitza, 1990] to improve its prediction capability since its first release in 1978. The most recent IRI model, IRI-2001, has presented a number of major improvements, including implementing new  $B0$  and  $B1$  tables to better determine the bottomside electron density profile [Bilitza *et al.*, 2000].

[3]  $B0$  and  $B1$  are parameters used to describe the thickness and shape of the profile. In earlier IRI versions, a standard  $B0$  table ( $B0$ -Tab) generated from profile inversion of ionograms at several stations was provided. An alternative table,  $B0$ -Gulyaeva, used Gulyaeva's model [Gulyaeva, 1987], which was based on the height of half maximum electron density  $h0.5$ . For  $B1$ , earlier IRI versions [Bilitza,

1990] took the constant value of 3. Comparisons with observations revealed large discrepancies in the bottomside density at various stations [e.g., Zhang *et al.*, 1996; Sethi and Pandey, 2001, and references therein], therefore there were various attempts to develop a new model for  $B0$  and  $B1$  [Huang and Reinisch, 1997; Adeniyi and Radicella, 1998; Mahajan and Sethi, 2001; Sethi *et al.*, 2000; Zhang *et al.*, 2000] through a series of IRI task force activities [Radicella, 2001]. Some of the results from these efforts have now been included in the newest IRI model, IRI-2001. In this model,  $B0$  tables were obtained from more ionosonde/digisonde stations using a sort of standard procedure, and now  $B1$  is assumed to be 1.8 during the day and 2.6 during the night to replace the constant value 3 used before. However, some discrepancies still exist between the IRI-2001 and measurements from ionosonde and incoherent scatter radar at low-mid latitude stations [e.g., Sethi and Mahajan, 2002]. It seems that analyzing more abundant databases (from various data sources and at different sites) to validate the IRI model is still useful and of great importance.

[4] The objective of the present paper is to report  $B0$ ,  $B1$  results from a carefully calibrated incoherent scatter radar (ISR) dataset for Millstone Hill (42.6°N, 288.5°E) covering more than two full solar cycles (1976–2002). A comprehensive picture of the diurnal, seasonal, and solar activity variation behavior of the two parameters will be discussed and used to assess the predictions of the IRI-2001.

## 2. Data Set and Analysis Method

[5] The Millstone Hill UHF ISR system operates with a zenith-directed 68 m diameter fixed parabolic antenna, which commenced operation in 1963, and a fully-steerable 46 m antenna, which commenced operation in 1978. More details about the ISR experiments and the data at Millstone Hill are given by Holt *et al.* [2002]. The archived data are downloaded from the Madrigal online database system (<http://www.openmadrigal.org>) hosted by Millstone Hill Observatory. A data set of about 70,304 electron height profiles measured by the zenith antenna for local measurements is analyzed in this study. They are grouped into three seasons, namely summer (May–August), winter (November–February), and equinox (March, April, September and October) under low ( $F107 < 150$ ) and high ( $F107 > 150$ ) solar activity, respectively. The mean  $F107$  is almost equal to 90 and 180 units in each season for low and high solar activity, respectively. Only data from magnetically quiet conditions with 3-hourly  $ap < 20$  are considered.

[6] First, the peak electron density ( $N_mF_2$ ) and its height ( $h_mF_2$ ) are obtained with a least-squares fitting of the

<sup>1</sup>Institute of Geology and Geophysics, Chinese Academy of Sciences, Beijing, China.

<sup>2</sup>Also at Wuhan Institute of Physics and Mathematics, Chinese Academy of Sciences, Wuhan, China.

<sup>3</sup>Also at Graduate School of the Chinese Academy of Sciences, Beijing, China.

<sup>4</sup>Haystack Observatory, Massachusetts Institute of Technology, Westford, Massachusetts, USA.

observed profile to the Chapman function [Rishbeth and Garriott, 1969],

$$N_e(h) = N_m F_2 \exp[0.5(1 - z - e^{-z})], \quad z = (h - h_m F_2)/H(h). \quad (1)$$

where the scale height is taken to be  $H(h) = A_1 (h - h_m F_2) + H_m$  for the bottomside, and  $H(h) = A_2 (h - h_m F_2) + H_m$  for the topside [Fox, 1994].  $N_m F_2$ ,  $h_m F_2$ ,  $H_m$ ,  $A_1$ , and  $A_2$  are variables to be adjusted. Our fitting is performed for profiles between 150 and 600 km with more than eight data points. Since  $B_0$  and  $B_1$  are parameters for the bottomside, to further secure reliable results, we have discarded the profiles with less than three points below the peak, as well as those fits with a logarithmic least squares deviation greater than 10%. The peak parameters  $N_m F_2$  and  $h_m F_2$  so derived generally look very reliable, as most fitted profiles nicely agree with the data [see also Fox, 1994].

[7] The thickness parameter  $B_0$  and the shape parameter  $B_1$  are obtained by fitting those observational profiles for which  $N_m F_2$  and  $h_m F_2$  can be determined in the first step. These fits are from  $h_m F_2$  down to the  $0.24 N_m F_2$  height ( $h_{0.24}$ ), with the formula used in the IRI model [Ramakrishnan and Rawer, 1972],

$$N_e(h) = N_m F_2 \exp(-x^{B_1}) / \cosh(x), \quad x = (h_m F_2 - h)/B_0. \quad (2)$$

[8] The recommended  $B$  parameters searching procedure is to constrain the fitting to the bottomside F2 region, i.e., from  $h_m F_2$  to  $h_{0.24}$  if the F1-layer does not exist, or to the F1 peak if it does. It is known that the F1-layer occurs most often in summer at low solar activity. Due to the limited height resolution in ISR data, however, it often becomes hard to correctly identify the F1-ledge. Therefore, our simple approach of using  $h_{0.24}$  should be considered valid under no F1 layer conditions or the F1 layer well below  $h_{0.24}$ . As is the case in many earlier studies, this approach may overestimate daytime  $B_0$  in summer, when the F1 layer frequently develops.

[9] It should be noted also that Millstone Hill ISR operates at various pulse modes providing different range resolutions. For this study, measurements with pulse length  $>640 \mu\text{s}$  are excluded. Most of the remaining data have pulse length  $300 \mu\text{s}$  or less with a height spacing of better than  $\sim 22$  km. There also are many data from multiple-pulse or alternating coded pulse measurements with a 4.5 km resolution. Using such a large dataset reduces the uncertainty in the results in a statistical sense. Still, the range smearing and coarse height resolution in the long-pulse data would result in systematic errors in  $B_0$  and  $B_1$  calculations if corrections were not made. So we have used data from a month-long experiment (October 2002) with simultaneously single pulse ( $480 \mu\text{s}$ ) and alternating code measurements to develop a detailed correction model for such errors. The  $B$  parameters from accurate alternating code data are compared to those from the  $480 \mu\text{s}$  data to determine the offset (correction). By making corrections which depend on pulse length under a linear assumption to pulse length, we finally obtain  $B_0$  and  $B_1$  values presented here.

[10] We also compare these results with those from the IRI-2001. The observed  $h_m F_2$ ,  $N_m F_2$  are used as inputs to

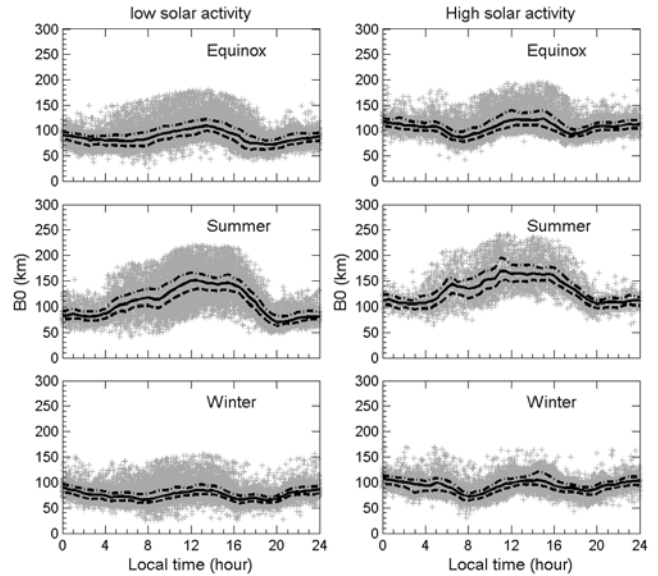


**Figure 1.** Diurnal and seasonal variation of the thick parameter  $B_0$  derived from Millstone Hill ISR observations under low and high solar activity. The median results are shown as solid lines; also included are the upper quartile, UQ (dash-dotted lines) and lower quartile, LQ (dashed lines) of  $B_0$  values.

IRI-2001 to compute  $B_0$  and  $B_1$  corresponding to each observed profile. Then a grouping process, the same as for the observed  $B_0$  and  $B_1$ , is performed to determine the model medians.

### 3. Results

#### 3.1. Experimental $B$ Parameters

[11] Figure 1 shows the diurnal variation of the thickness parameter  $B_0$  against local time under low and high solar activities; the corresponding median values, upper quartile (UQ) and lower quartile (LQ) are also given. The results show a large day-to-day variation in all seasons. The value of  $B_0$  is lower at night and higher during the day, while its detailed variation pattern changes with season and solar activity. We concentrate on the variations of median  $B_0$  for low solar activity. In equinox,  $B_0$  increases from its nighttime value of  $\sim 70$  km to a diurnal peak of  $\sim 110$  km at 13 LT, and then falls gradually until 17 LT. In summer,  $B_0$  begins to enhance at 03 LT, and reaches its peak values of 140 km between 12–16 LT followed by a tendency of decrease. In winter, the maximum value also occurs at 13 LT as in equinox, while the diurnal variation of  $B_0$  is characterized by morning and afternoon collapses, which are, however, somewhat weak in the equinox and almost absent in summer. Thus the minimum  $B_0$  in winter occurs in the morning instead of at night. Additionally, the daytime  $B_0$  is higher in summer and lower in winter, while the nighttime  $B_0$  does not show an evident seasonal effect. Further, the day-to-night difference is large in summer and very small in winter.

[12] For high solar activity, the diurnal and seasonal variations of  $B_0$  are somewhat similar to those under low solar activity, but the morning collapse becomes more

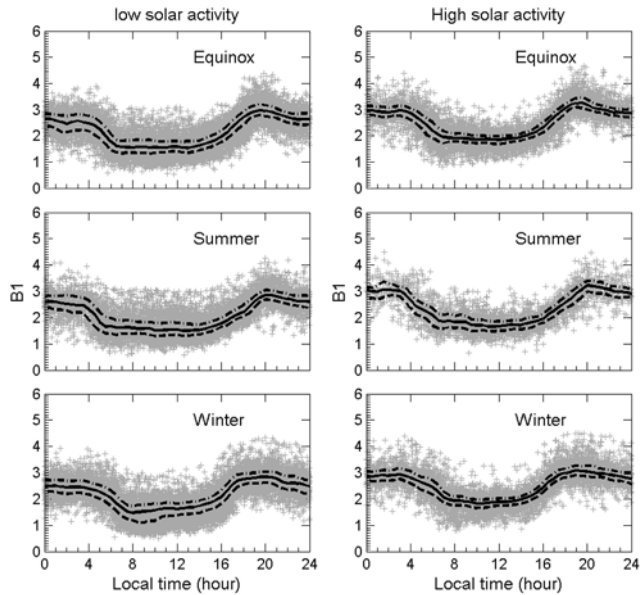


**Figure 2.** Same as Figure 1, except for the shape parameter  $B1$ .

evident here. Also, the nighttime values are lower by around 10 km in winter than in the other two seasons. It is interesting to note that the morning collapse of  $B0$  is also found at Arecibo, a low latitude station, while the afternoon one is absent [Sethi and Mahajan, 2002]. From low to high solar activity, as seen from Figure 1,  $B0$  increases by about 30% during the night and by about 20% during the day, except for the morning collapse periods in equinox and winter when  $B0$  increases by less than 10%. As a result, the morning collapse under high activity is more pronounced, as mentioned previously.

[13] Figure 2 presents a scatter plot of the shape parameter  $B1$  against local time under low and high solar activities along with the corresponding median values. It can be observed that  $B1$  shows a large scatter, with values varying between 0.8 and 5. The solar activity dependence of  $B1$  is similar to that of  $B0$ , yet the diurnal as well as seasonal dependences are different. The diurnal variation pattern of the  $B1$  median is very simple: lower by day with a value of  $\sim 1.7$  (1.9) and higher at night with a value of  $\sim 2.5$  (2.9) under low (high) solar activity. For the seasonal variation, it is higher in winter and lower in summer during the day, but has no obvious seasonal variation at night. It increases by  $\sim 15\%$  from low to high solar activity. This solar activity dependence is consistent with that of Zhang *et al.* [2000], but opposite to that found at Arecibo [Sethi and Mahajan, 2002]. The latitudinal variation of its solar activity dependence needs further investigation.

### 3.2. Comparison With IRI Model

[14] Figure 3 shows a comparison of the median  $B0$  obtained from fitting observed density profiles with that predicted by the IRI-2001. The uncertainty of the observed  $B0$  is represented by error bars covering the range from the LQ to the UQ through the median. It can be seen that  $B0$ -Gulyaeva values agree with the observations in the diurnal tendency, but they tend to be lower by 10–20 km under high solar activity. The new  $B0$ -Tab values seem less

variable in the diurnal course, giving smaller day-night differences and showing no morning and afternoon collapses. Generally, the diurnal curves predicted by both IRI options are somewhat symmetric to local noon, while this symmetry is not very clear in experimental values. For the solar activity dependency, the  $B0$ -Tab values increase from low to high solar activity by a larger percentage than observed results do. In summer under low solar activity, the observation is fairly high as compared to any of the IRI values, and, as mentioned earlier, these differences may be attributed to various definitions of the starting height in fitting for the  $B$  values such that the extent of contamination of the F1 layer occurrence differs.

[15] Figure 4 shows a comparison of the experimental  $B1$  values with that of IRI.  $B1$ -Tab values are generally close to the experimental values for high solar activity during the day, while they are proximate to the observations for low solar activity at night, except for the sunset period ( $\sim 18$ – $21$  LT), when the  $B1$ -Tab values are much lower than the two groups of the experimental ones. The experimental  $B1$  increases by as much as  $\sim 15\%$  from low to high solar activity, however, IRI does not give any solar activity dependence, which was also noted by Sethi and Mahajan [2002].  $B1$ -Gulyaeva values generally agree with the observed ones for high solar activity during nighttime, while they are significantly larger during daytime than those from the measurements, given that the  $B1$ -Gulyaeva option takes the constant value of 3, not subject to changes with local time, season and solar activity.

## 4. Summary and Conclusions

[16] The incoherent scatter radar measurements over Millstone Hill during 1976–2002 have been used to inves-

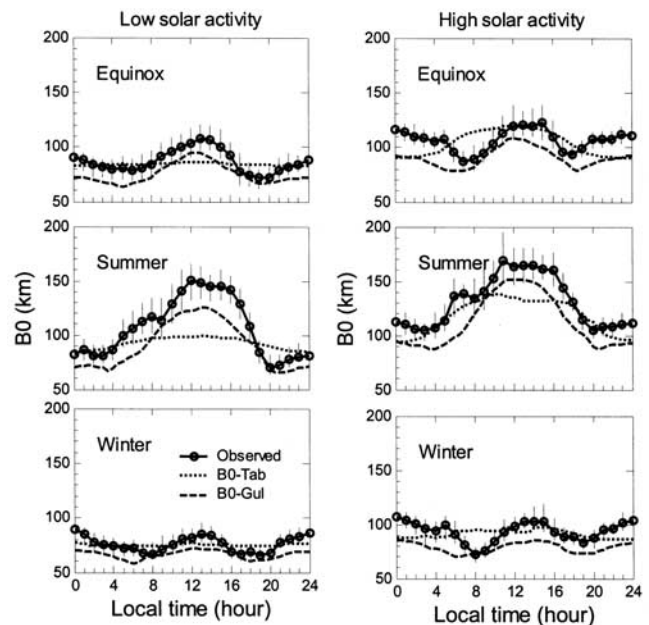


**Figure 3.** Comparisons of the median values of  $B0$  obtained from the Millstone Hill ISR measurements with  $B0$ -Tab (dotted lines) and  $B0$ -Gulyaeva (dashed lines) values predicted by the IRI model. The vertical bars cover UQ through median values to LQ.

